

<https://doi.org/10.1038/s44328-025-00063-w>

# Ad hoc manufactured OECT glucose sensor in capillary-driven microfluidic



Bernhard Burtscher<sup>1</sup>, Chiara Diacci<sup>1</sup>, Pooya Azizian<sup>2</sup>, Marios Savvakis<sup>1</sup>, Tobias Abrahamsson<sup>1</sup>, Joan M. Cabot<sup>2</sup>, Xenofon Strakosas<sup>1</sup> ✉ & Daniel T. Simon<sup>1</sup> ✉

Glucose sensors are essential for managing diabetes, a metabolic disease affecting 1 in 10 adults globally. Enzyme-based biosensors, particularly those utilizing oxidoreductases, offer high specificity for glucose detection. This study explores the use of flavin-dependent glucose dehydrogenase from *Aspergillus oryzae* (AoGDH) in developing glucose sensors integrated into organic electrochemical transistors (OECTs) without mediators. We employed tri-thiophene monomer units to form conductive polymers interfacing with AoGDH, allowing sensing due to the proximity of the FAD cofactor. Despite AoGDH's lower stability compared to glucose oxidase (GOx), its ability to function without oxygen sensitivity makes it advantageous. Using electropolymerization, we successfully incorporated AoGDH into the OECT gate electrode, demonstrating glucose detection in physiological ranges, albeit in buffer solutions. Furthermore, integrating this system into a 3D-printed capillary-driven microfluidic device facilitated on-demand sensor fabrication, enhancing portability and point-of-care application potential. This study underscores the viability of AoGDH-based, and ad hoc fabricated, OECT sensors for accurate and responsive glucose monitoring in biomedical applications.

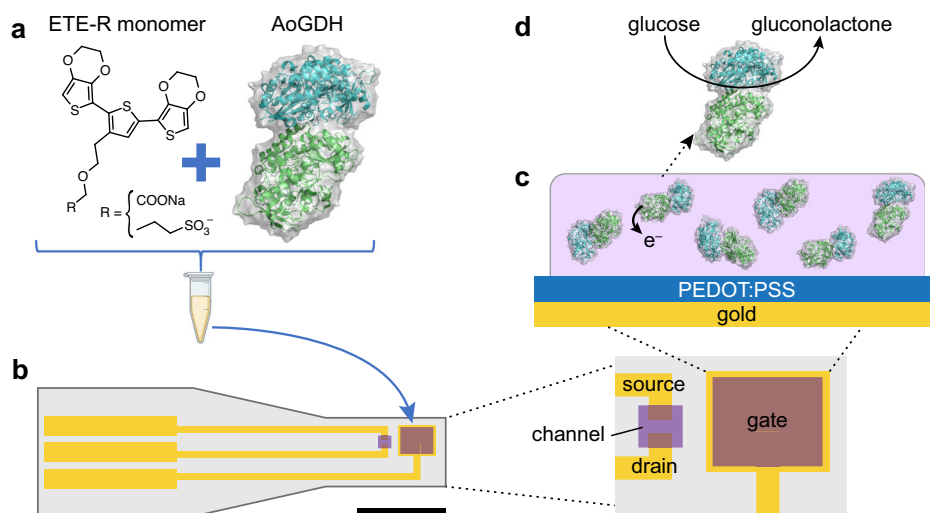
Glucose sensors are a heavily studied and well-developed technology since they provide a necessary tool in both hospitals and at point-of-care to monitor diabetes, a metabolic disease that affects 1 in 10 (aged 20–79 in 2021), with incidence only increasing<sup>1</sup>. Glucose levels are maintained in a small window (3.5–6 mM) and even a slight increase (7 mM) can be a sign of diabetes in fasting blood glucose levels<sup>2–4</sup>.

Enzymes are extensively used to develop biosensors for metabolite detection because of their ability to catalyze the conversion of highly specific substrates – i.e., analytes – into products. Oxidoreductases specifically are involved in the reduction and oxidation of substrates, transferring electrons through the enzymatic cofactor from substrate to product, making them a highly attractive sensing unit for selective electronic biosensors<sup>5,6</sup>. The electron transfer (ET) to the biosensor's electrode surface can occur with three different mechanisms, depending on the enzyme structure, modification, and/or functionalization method: (i) the enzymatic reaction produces electroactive species that are oxidized/reduced at the electrode (e.g., H<sub>2</sub>O<sub>2</sub>); (ii) the enzymatic reaction uses a redox mediator to shuttle the electron from the cofactor site to the electrode surface, often referred to as mediated electron transfer; (iii) the enzymatic reaction produces electrons which can be transferred directly to the electrode, due to the cofactor's proximity with the surface. Sensors, based on the final enzymatic mechanism, are referred to as direct electron transfer (DET) or “3<sup>rd</sup> generation”<sup>5</sup>.

Creating a 3<sup>rd</sup> generation enzymatic sensor comes with a set of problems<sup>5</sup>. Oxygen sensitivity, as an electron acceptor, is one of these problems for most enzymes and can be circumvented by selecting a dehydrogenase enzyme, such as flavin-dependent glucose dehydrogenase (FAD-GDH) instead of glucose oxidase (GOx)<sup>7</sup>. GOx is one of the most frequently used enzymatic units to detect glucose, but current approaches in 3<sup>rd</sup> generation configurations are debated as wiring the cofactor (facilitating electron transfer) directly to the electrode is not straightforward and may not be possible at all<sup>5,8–10</sup>. This is because the GOx structure presents a homodimer (two flavin adenine dinucleotide, FAD, sites) protected deeply inside the enzyme pocket, thus far from the surface and the electrodes (17–22 Å)<sup>11–13</sup>. This distance is also increased by the high glycosylation of the enzyme, making electron tunneling to the electrode highly improbable for GOx<sup>9</sup>. An alternative is FAD-GDH, a dehydrogenase enzyme derived from fungi, bacteria, or insects<sup>7</sup>. Depending on the type and source of enzyme, different subunits present a cofactor close to the surface (e.g., heme), so no mediated pathway is needed to achieve electron transfer (Fig. 1c). It should be noted that present bacteria-derived FAD-GDH often have affinity for maltose and fungi-derived FAD-GDH have affinity for xylose, though new derivatives with less interference are actively researched<sup>6,7</sup>. Secondary substrates can cause interference and limit biosensor applications, so must be controlled for, if present<sup>6,7</sup>. FAD-GDH is most often found in fuel cell demonstrations, but has also been used for amperometric biosensors<sup>7,14–16</sup>.

<sup>1</sup>Laboratory of Organic Electronics, Department of Science and Technology, Linköping University, Norrköping, Sweden. <sup>2</sup>Diagnostic devices, Digital Industry Department, LEITAT Technological Center, Terrassa, Barcelona, Spain. ✉e-mail: [xenofon.strakosas@liu.se](mailto:xenofon.strakosas@liu.se); [daniel.simon@liu.se](mailto:daniel.simon@liu.se)

**Fig. 1 | Functionalization of PEDOT:PSS-based OECT.** **a** Polymerization cocktail containing monomer (ETE-COONa or ETE-S) and enzyme. **b** Polymer matrix with enzymes formed on top of PEDOT:PSS gate electrode and **c** zoom of electron transfer into polymer matrix. Scale bar 500  $\mu\text{m}$ . **d** Schematic of a potential electron pathway. AoGDH structure created in PyMol.



In this study, we used a commercial FAD-GDH linked to *Aspergillus oryzae* by Milton et al.<sup>17</sup>. *Aspergillus oryzae* FAD-GDH (AoGDH) has no heme cofactor<sup>18</sup> and therefore the mechanism for electron transfer from FAD to the electrode is of a different origin. It has been speculated to be direct tunneling/transfer<sup>19</sup>, and glucose could thus be sensed without a mediator. AoGDH has an entrance in the protein data bank (PDB ID: 7VZP)<sup>20</sup>, where X-ray experiments indicate that the FAD is around 13 Å inside the enzyme (center, not edge of the FAD). The direct electron transfer mechanism, and therefore 3rd generation sensor with AoGDH, was corroborated by another work where glucose was sensed without a mediator due to the proximity of debundled single-walled carbon nanotubes to the enzymes (no glucose response was observed if the carbon nanotubes were bundled)<sup>21</sup>. In general, there have been several approaches to facilitate enzyme ET, and finding or engineering a more accessible cofactor close to the surface is one promising strategy (as in the case of FAD-GDH). Others have proposed methods including enzyme orientation, immobilization of cofactors on the surface, using structures that can penetrate to the active site of the enzyme, or immobilization into a preformed matrix, to name a few<sup>6,7,15,22</sup>.

Another piece of the puzzle in biosensor development is enhancing the electrical signals used to determine analyte concentration. Transistor-based biosensors have thus gained wide interest, with electrolyte-gated transistors (and organic electrochemical transistors, OECTs, in particular) taking a leading role. In general, transistors are three-terminal devices in which a current flow between the two terminals of a semiconductor channel is regulated (“amplified”) by a third terminal, controlling the amount of current passing through the semiconductor. For OECTs, the organic mixed ionic-electronic conductor (OMIEC) channel layer and the gate are coupled by an electrolyte (instead of the dielectric of field effect transistors), and a voltage at the gate electrode pushes ions from the electrolyte into the channel layer<sup>23,24</sup>. By far the most common OMIEC used for OECTs is the conducting polymer/polyelectrolyte blend poly(3,4-ethylenedioxythiophene) doped with polystyrene sulfonate (PEDOT:PSS). For a depletion-mode p-type PEDOT:PSS channel, cations driven into the OMIEC channel (*i.e.*, by positive gate voltage) charge-balance the sulfonate groups on the PSS and therefore reduce the doping state of PEDOT. This switches the transistor “off”, hence the classification as depletion mode. Since the OMIEC channel exhibits bulk ion conductivity and thus bulk electrochemical activity, OECTs are defined by scaling with the channel volume, not only the channel surface area, enabling demonstration with high transconductance ( $\partial I_{DS}/\partial V_{GS}$ , where  $I_{DS}$  is the drain current through the OMIEC channel and  $V_{GS}$  is the gate voltage). Generally, faradaic and non-faradaic principles are distinguished in OECT biosensors. Non-faradaic or capacitive sensors feature no electron transfer but rely on capacitive changes at one or more

interfaces. On the other hand, faradaic sensors exhibit charge transfer when electrons from the solution (e.g., from an enzyme) cross the electrolyte/electrode interface.

Enzymes are commonly used recognition elements to add specificity/selectivity to OECT<sup>25</sup> and field effect transistor biosensors<sup>26</sup>. Enzyme-based OECT sensors are also able to sense in complex solutions, e.g., plant xylem sap<sup>27</sup> or cells<sup>28</sup>. Drop casting the enzymes on the gate or channel surface remains a common approach<sup>28–31</sup>. Though drop casting is simple, the orientation of the enzyme is random, and the enzyme can easily detach from the surface. While binding to the surface is possible, orienting the enzymes into the most favorable enzyme/electrode complex is equally important<sup>9,32</sup>. Another solution is the integration into a polymer matrix (ideally conductive).

For our approach, we utilize tri-thiophene monomer building blocks (Fig. 1a) to form PEDOT- and polythiophene-like polymers interfacing with AoGDH for glucose sensing. These monomers have shown great potential in interfacing with enzymes<sup>33–35</sup> and forming conducting polymers in living animals<sup>33,36</sup>. Furthermore, due to their OMEIC nature, they can be used for OECT applications<sup>37</sup>. Here, we utilized the in situ polymerization of monomers in solution with enzymes to form a polymer/enzyme matrix. The (electro)polymerization could be achieved at low potentials and could even be driven by enzymatic reactions, as has been shown for similar monomers<sup>33–35</sup>.

While FAD-GDH offers a viable solution to circumvent the oxygen sensitivity of GOx, it has shown lower stability, which has limited its applicability. As a solution to this issue, we suggest an ad hoc fabrication inside a microfluidic device, which still allows for a portable measurement platform. Microfluidics has been shown to not only be a convenient augmentation to biosensor systems, but also a possible option to aid detection<sup>30,38</sup>. Microfluidic devices mostly operate using external flow actuators, whereas capillary-driven microfluidics use capillary action to regulate and drag the liquid along the designed microchannels. These systems are passive and do not need peripheral equipment like electrically powered valves and pumps, so they are a sustainable alternative and ideal for point-of-care applications<sup>38</sup>. Furthermore, employing 3D features allows the sophisticated possibility of sequencing capillary flows<sup>39</sup>, for which 3D printing has enabled highly customizable microfluidics, allowing more complex structures to be produced for biomedical applications<sup>40,41</sup>.

## Results and discussion

The monomer system referred to above is based on functionalized varieties of an EDOT-thiophene-EDOT (“ETE”) unit, where EDOT is the 3,4-ethylenedioxythiophene monomer of PEDOT (Fig. 1a). In this study, we focused on OECT structures functionalized with various ETE-enzyme

cocktails. To form a homogenous layer, electropolymerization (chronoamperometry) was used to form an enzyme-polymer matrix from an enzyme/monomer solution on the gate electrode of a PEDOT: PSS-based OECT (Fig. 1a–c); i.e., a premade Au-contact OECT with PEDOT: PSS channel and gate electrode (see materials and methods). This general structure was designed to provide a system where, if the AoGDH has a cofactor close to the surface of the enzyme (Fig. 1c), electron transfer would be possible directly into the polymer matrix.

Monomers with different side groups have been used successfully in combination with enzymes but have shown slight variations in properties, e.g., polymerization potential<sup>35</sup>. We chose two main candidates, ETE-S and ETE-COONa (Fig. 1a), and analyzed their cyclic voltammetry after film formation, with and without enzymes (Fig. 2a). Clean ETE-COONa films (no enzyme) exhibited a reductive current in a similar range where one would expect FAD activity ( $-0.265$  V vs SHE or  $-0.45$  V vs Ag/AgCl)<sup>42</sup>. Similar behavior was observed for ETE-S and ETE-S with AoGDH. Because of the polymers' reduction currents, AoGDH peaks were difficult to identify. Both pETE (polymer) varieties without enzyme showed a similar box shape from  $-0.1$  V to  $0.2$  V. But with enzymes, the capacitance (area inside CV curve) reduces slightly for pETE-S/AoGDH, whereas the capacitance increases slightly for pETE-COONa/AoGDH.

Figure 2b shows the current response ( $I_{DS}$ ) of an OECT with a pETE-COONa/AoGDH film on top of the PEDOT: PSS/Au gate electrode. After an initial stabilization time, various glucose concentrations (from  $100$   $\mu$ M to  $40$  mM) were added and the sensor response observed. Upon each glucose solution change, a current increase was observed (Fig. 2b with concentration change indicated). In most cases, the response seemed rather slow and linear after glucose addition (up to  $20$  mM), with no step-like behavior. Both pETE-S and pETE-COONa with AoGDH combinations were tested in a constant OECT configuration (recording  $I_{DS}$  vs time) to measure glucose levels. pETE-COONa/AoGDH outperformed pETE-S/AoGDH significantly, with the disparity increasing with concentration up to nearly an order of magnitude at  $40$  mM. The measured signal is expressed as normalized response,  $NR = (I_x - I_0)/I_0$ , where  $I_x$  is the current at  $x$  M glucose just before the next concentration is added and  $I_0$  is the current without glucose before the first addition. Repetition of the experiments revealed that pETE-COONa/AoGDH outperforms pETE-S/AoGDH again (with varying disparity, Fig. S2), therefore, pETE-COONa/AoGDH was chosen to investigate

in more detail. The disparity between the two trimers could be that in the case of pETE-COONa/AoGDH, the conductive part of the formed polymer is more favorably oriented in relation to the enzyme cofactor than in the case of pETE-S/AoGDH. We also performed a comparison measurement with GOx embedded in the pETE-COONa instead of AoGDH (Fig. 2d). Only the combination with AoGDH resulted in an observable glucose response in the range  $2$ – $40$  mM. While sensing glucose by incorporating GOx into the matrix was not successful, production of  $H_2O_2$  could still occur, and therefore we investigated the effect of  $H_2O_2$  on the OECT, which was negligible (Fig. S3).

In order to more deeply assess our strategy's viability for biosensing, different monomer to enzyme ratios and polymerization times were investigated (Fig. S4). Reproducibility was also tested and the corresponding dose curve for 4 samples can be seen in Fig. 3a. To show that it follows a typical enzyme trend, it was fitted with a sigmoid function as a visual guide<sup>43</sup>. Levels corresponding to normal/healthy blood glucose concentration are indicated in green and elevated/warning levels in orange, showing that our sensor covers this range nearly perfectly over its linear range (albeit in buffer solution). In Fig. 3b we investigated the effect of gate potential on the normalized response and found that lower gate potentials (even  $0$  V and  $0.1$  V) were also able to detect glucose. Their signal response was comparable to that of  $0.3$  V or  $0.5$  V. While surprising at first glance, especially when considering mediated electron transfer, in DET, the only redox potential to be overcome is the one from FAD. For cyclic voltammetry, an overpotential of  $+0.1$  V relative to the potential of the FAD ( $-0.45$  V vs Ag/AgCl) was calculated to indicate a tunneling distance of approximately  $1$  nm<sup>21</sup>. Another consideration stems from the OECT setup and its undefined electrochemical nature. Often, no reference electrode is employed, and therefore, only relative voltage differences are considered rather than the absolute voltage in the system. Another issue to consider is that while  $V_{GS}$  might be small, there is also  $V_{DS}$  to consider, and therefore an implicit difference.

One drawback is that AoGDH seems to be less stable than GOx, and Fig. 3c also shows a significant decrease in normalized response ( $10\times$  for  $4$  mM) after 7 days, effectively losing sensitivity in the physiological region of ( $3.5$ – $6$  mM). Though it should be noted that for this sample, the monomer/enzyme solution was 3 days old at day 0, indicating that storage of the solution exhibits slower degradation than storage of the formed sensor. Continuous glucose monitoring technology is also limited by storage and

**Fig. 2 | Comparison of monomer/enzyme mixes.**

**a** Cyclic voltammetry of pETE-S and pETE-COONa films with and without AoGDH. **b** OECT measurement ( $I_{DS}$  vs time) during sequential additions of increasing glucose concentration. (i:  $100$   $\mu$ M, ii:  $200$   $\mu$ M, iii:  $300$   $\mu$ M, iv:  $500$   $\mu$ M, v:  $700$   $\mu$ M, vi:  $1$  mM, vii:  $2$  mM, viii:  $4$  mM, ix:  $10$  mM, x:  $20$  mM, xi:  $40$  mM). **c** Comparison of OECT glucose sensing with pETE-S/AoGDH and pETE-COONa/AoGDH films. **d** Comparison of sensing with pETE-COONa without enzyme, with GOx, and with AoGDH.

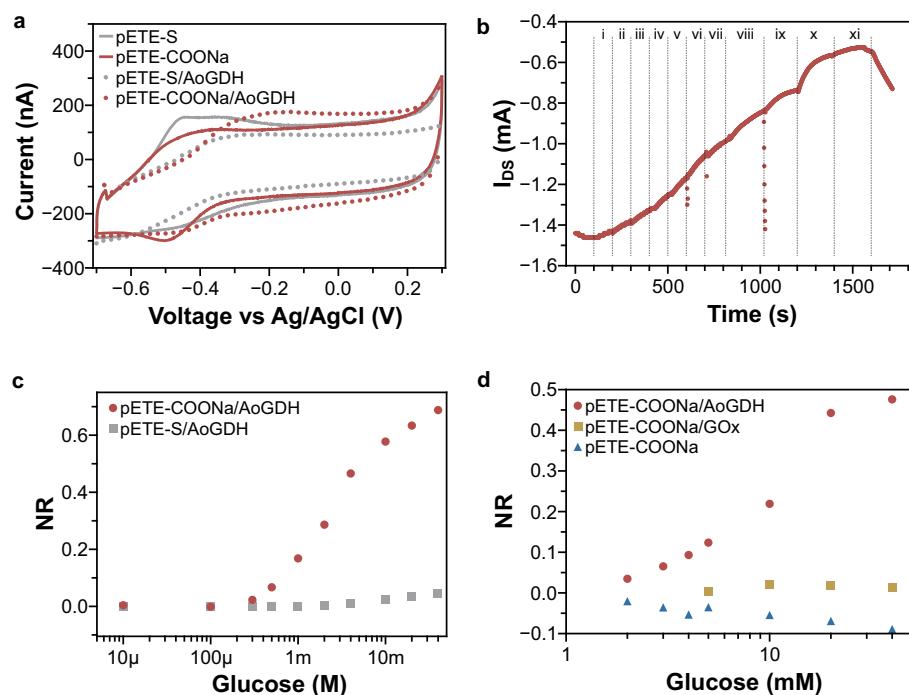


**Fig. 3 | Characterization and stability of pETE-COONa/AoGDH OECT sensing.** **a** NR vs concentration (for four devices) and sigmoid fit as eye-guide. Green and orange bars indicated healthy and problematic blood glucose levels. **b** Effect of different gate voltages on the normalized response. **c** Effect of storage on sensor response with sigmoid function as eye-guide.

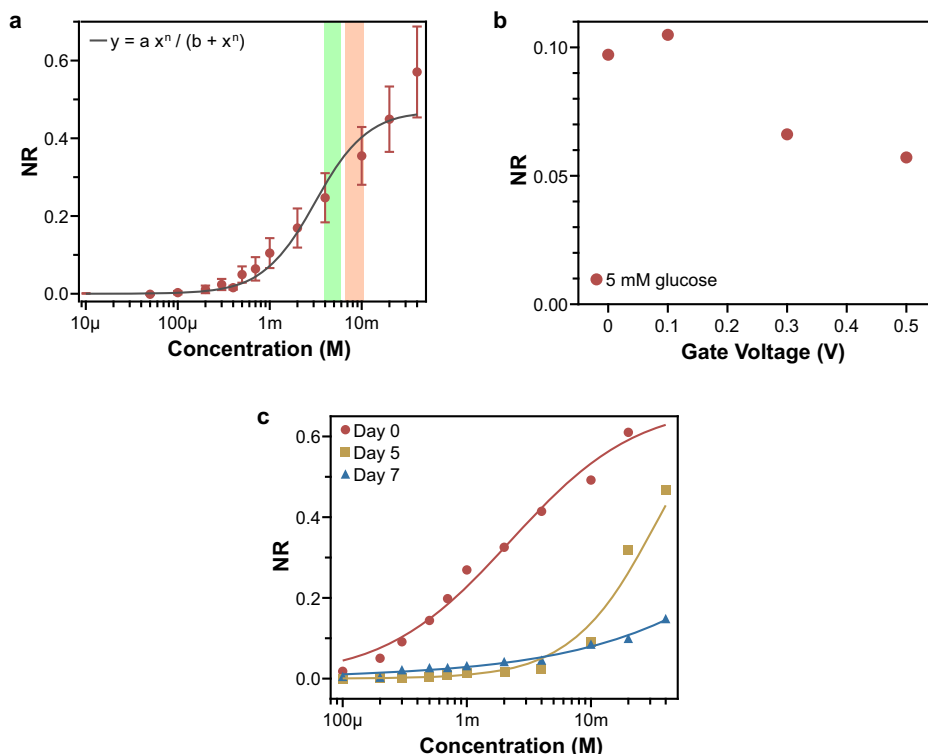
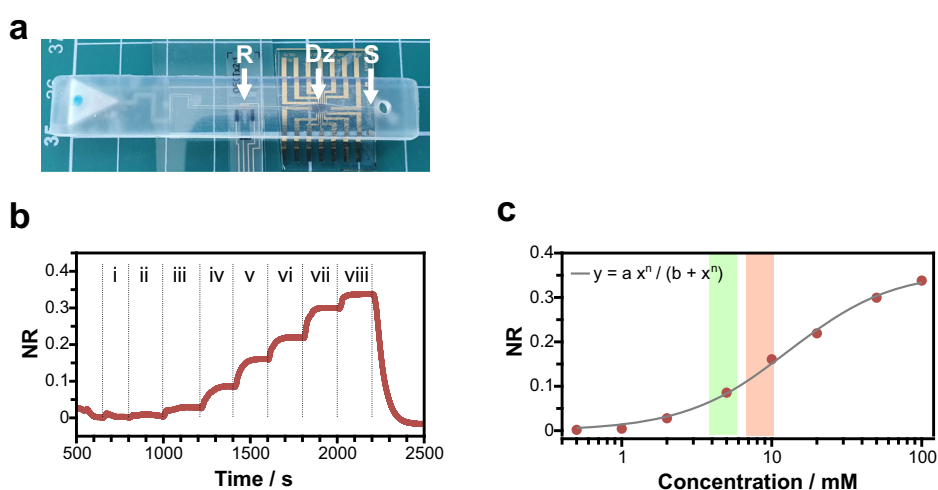


**Fig. 4 | Ad hoc OECT sensor coupled to microfluidic.** The assembled OECT with a capillary-driven microfluidic device having a retention valve S (a), sensor curve example (b; glucose concentration: i: 500  $\mu$ M; ii: 1 mM, iii: 2 mM, iv: 5 mM, v: 10 mM, vi: 20 mM, vii: 50 mM, viii: 100 mM) and dose curve inside microfluidic (c) VDS =  $-0.3$  V; VGS =  $0.3$  V. A sigmoid fit is given as an eye guide.



degradation, which also constrain fabrication and shipping times for a sensing product. Given the relative ease of functionalization of our approach by electropolymerization, an ad hoc fabricated sensor inside a capillary-driven microfluidic device can be realized.

To couple the OECT with a microfluidic device, we fabricated Au-contact OECTs with PEDOT: PSS on the channel and gate electrode on a glass substrate. A thin double-sided adhesive tape allowed for the attachment of the 3D printed microfluidic to the glass substrate. The reference electrode (R in Fig. 4a) for electropolymerization was a separate screen-printed electrode integrated with the microfluidic. For the first tests, we used a microfluidic design with a single inlet with determined resistance (capillary retention valve, marked S) to prevent emptying of the microchannel (Figs. 4a, 5). Thus, the liquid at the inlet would stop after the inlet reservoir (having filled the microfluidic channel) and adding another drop into this reservoir would continue the fluid flow in the microfluidic channel. With

this passive stop-and-go approach, functionalization, washing, and measuring of glucose could be performed on demand.

The microfluidic was tested with DI water for leakage before adding the monomer/enzyme solution, filling the detection zone (Dz) with the OECT, and the patch for the reference electrode (R). The gate electrode was then functionalized as above using chronoamperometric electropolymerization. The system was then washed with PBS 1 $\times$  buffer and the measurement ( $I_{DS}$  vs time) for glucose concentration (0.5–100 mM) obtained (Fig. 4b). The physiological range of interest can be resolved, as seen by the step for 5 mM of glucose (iv) as well as in the dose curve (Fig. 4c). This system shows a lower response to the same concentrations compared to the open OECT measurements above (Fig. 3a), possibly due to polymerization inside the microfluidic. The lower reservoir volume during polymerization or the electrodes being connected via small liquid channels (thus introducing resistance) could affect the polymerization and therefore the dose curve.

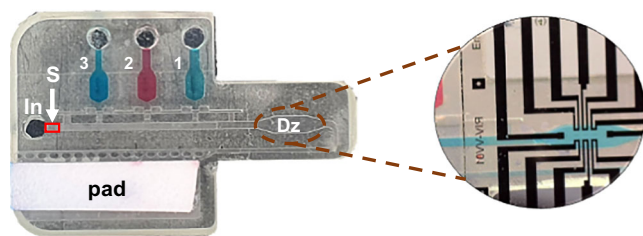


**Fig. 5** | Envisioned microfluidic device with preprogrammed sequence (scalebar = 10 mm) and its integration with an OECT (zoom; scalebar = 4 mm).

An envisioned version with an “automated” release sequence of reservoirs (1-3) is shown in Fig. 5, based on a previously described principle<sup>39</sup>. This allows not only for a preprogrammed sequence to occur but also limits unwanted diffusion from the reservoirs to the microchannel. Figure S5 depicts the time evolution of the microfluidic device for an automated delivery of reagents in a preprogrammed sequence. Coupling the on-demand fabrication with the fact that OECTs can be operated with microcontroller systems<sup>29</sup> makes this valuable for point-of-care approaches (Fig. S5b), with the added benefit of microfluidics only requiring small sample volumes.

We have demonstrated ad hoc fabrication of OECT-based glucose sensors with enzymes embedded in a polymer matrix on the channel. The system exhibits easy and targeted fabrication even within a microfluidic channel. The recognition element is the enzyme AoGDH, and to the best of our knowledge, this is the first report of AoGDH in an OECT-based sensor (but FAD-GDH has been integrated with other transistor sensors<sup>44</sup>). Due to the uncertainty of the origin species of the commercial enzyme, only tentative statements on the transfer mechanism can be drawn, even though glucose could be measured without mediator. This was not the case for GOx with the same approach. Also, given the significance of the origin of the possible electron transfer mechanism (even 3<sup>rd</sup> generation), a clear indication of its origin should be provided if possible, to avoid misunderstandings. This is especially important as some FAD-GDH species have been investigated more than others, and their structures are therefore better understood. Likewise, OECTs have been used with capillary-driven microfluidics for ion sensing<sup>45</sup> or with finger-powered microfluidics for enzymatic sensing<sup>46</sup>, but we believe this to be the first demonstration of such a system fabricated/functionalized on demand inside the fluidic channel.

This ad hoc fabrication allows us to circumvent a drawback of FAD-GDH sensors: their stability. The physiological concentration range was clearly detectable within the microfluidic setup. In addition, a fast reaction time of the sensor was achieved, visible as a step-like behavior on analyte addition. Furthermore, an “automated” release sequence of reagents inside the microfluidic channel can be preprogrammed by including more reservoirs with different retentions at their upstream (reservoir inlets). The special design of the reservoirs’ connections to the main microfluidic channel mitigates premature intermixing and diffusion<sup>39</sup>.

Further investigation to reduce device-to-device variation in glucose detection is crucial for a reliable conclusion of glucose levels. Multiple sequential film formations are possible, potentially expanding the operation time of the device and possibly allowing for near continuous monitoring. Furthermore, given the targeted deposition onto electrodes, a multi-electrode sensing array can also be envisioned.

## Methods

Chemicals were obtained from Sigma Aldrich unless otherwise stated. FAD-GDH was purchased from BBI solutions. ETE-S and ETE-COONa were synthesized as described previously<sup>33</sup>.

For flexible OECT, photolithography was used to fabricate OECTs on PET foil, followed by the same process as described previously<sup>29,47</sup>. The channel width is 100  $\mu\text{m}$ , the length is 20  $\mu\text{m}$ , and the gate is 250  $\times$  250  $\mu\text{m}$ .

For integration with capillary-driven microfluidic devices, micro-fabricated OECTs were fabricated with a double Parylene C layer on glass

slides with Cr (5 nm) and Au (50 nm) trough photolithography as previously described<sup>23</sup>. PEDOT: PSS films were spin-coated (1400 rpm for 30 sec) and cured for 1 h at 120  $^{\circ}\text{C}$  before removing the sacrificial Parylene C layer. Channel width is 100  $\mu\text{m}$ , length is 10  $\mu\text{m}$ , and the gate is 600  $\times$  600  $\mu\text{m}$ . PEDOT: PSS formulation consisted of PH1000 with 5% ethylene glycol (v/v), 1% (3-glycidyloxypropyl)trimethoxysilane (GOPS, v/v), and dodecylbenzenesulfonic acid (DBSA, 1 drop per 5 ml).

ETE-COONa (1 mg/ml) was mixed with AoGDH (5 mg/ml) in PBS 1 $\times$  and polymerized onto an electrode with 300 mV for 60 sec in a two-electrode setup with an Ag/AgCl as counter/reference electrode. For devices in microfluidic chips, a screen-printed Ag/AgCl was used<sup>48</sup>.

## Measurement strategy

Electrical characterizations were performed using a Keithley 2612 and a custom LabVIEW program. Or in the case of integration with the microfluidic chip, a microcontroller was used as described by Diacci et al.<sup>29</sup>. Cyclic voltammetry and chronoamperometry were obtained using a Keithley 2612 with a custom LabVIEW program and Ag/AgCl as reference electrode (pellet for free-standing or screen-printed for microfluidic integration) in a 2-electrode setup. The normalized response (NR) of the sensor upon glucose addition was taken before changing to another concentration and calculated via  $NR = (I_x - I_0)/I_0$ , with  $I_x$  the current at a given concentration  $x$  and  $I_0$  the current without glucose (before addition of glucose).

## Capillary-driven microfluidics

The microfluidic devices were designed with SolidWorks 2021 (Dassault Systèmes SE, France) and printed using the stereolithography (SLA) 3D printer Form3 (Formlabs, USA). Clear V4 resin was used in all cases. After 3DP, they were activated by atmospheric plasma (Plasmatreat Steinhagen FG3001 + RD1004, Germany). A 1.6-mm-thick optically clear silicone pressure-sensitive adhesive (PSA) was used to seal the microchannels (ARclear 93495, Adhesives Research, Ireland). Subsequent to plasma activation of the 3DP chips, the results showed hydrophilicity with the contact angle of  $30^{\circ} \pm 5^{\circ}$  for over a week, whereas the sealing layer of PSA was hydrophobic (C.A.  $\sim 100^{\circ}$ ). As the utilized PSA is a double-sided adhesive, it attaches the microfluidic chip with the reference electrode and micro-fabricated OECT on a glass slide, while the shapes and openings were cut with a cutting machine (Cricut Explore 3). We found that having “ripples” in the detection zone was beneficial compared to a flat surface to facilitate a homogeneous filling of the chip without air bubbles.

Alignment of the microfluidic chip, the adhesive silicone, and the OECT was done manually. During the mounting of the OECT with a Parylene C encapsulation layer on glass, this encapsulation layer around the gate was damaged, increasing the functionalized gate area for the measurement in Fig. 4.

## Data availability

The authors declare that the data supporting the findings of this study are available within the paper and its Supplementary Information files. Should any raw data files be needed in another format they are available from the corresponding author upon reasonable request.

Received: 17 March 2025; Accepted: 1 November 2025;

Published online: 04 December 2025

## References

1. Sun, H. et al. IDF Diabetes Atlas: Global, regional and country-level diabetes prevalence estimates for 2021 and projections for 2045. *Diabetes Res. Clin. Pract.* **183**, 109119 (2022).
2. Zhou, B. et al. Worldwide trends in diabetes since 1980: a pooled analysis of 751 population-based studies with 4.4 million participants. *Lancet* **387**, 1513–1530 (2016).
3. Hindmarsh, P. C. & Geertsma, K. Glucose and Cortisol. in *Congenital Adrenal Hyperplasia* 219–230 (Elsevier). <https://doi.org/10.1016/B978-0-12-811483-4.00019-2> 2017.

4. Güemes, M., Rahman, S. A. & Hussain, K. What is a normal blood glucose?. *Arch. Dis. Child.* **101**, 569–574 (2016).
5. Milton, R. D. & Minter, S. D. Direct enzymatic bioelectrocatalysis: differentiating between myth and reality. *J. R. Soc. Interface* **14**, 20170253 (2017).
6. Bollella, P. Enzyme-based amperometric biosensors: 60 years later ... Quo Vadis?. *Anal. Chim. Acta* **1234**, 340517 (2022).
7. Okuda-Shimazaki, J., Yoshida, H. & Sode, K. FAD dependent glucose dehydrogenases - Discovery and engineering of representative glucose sensing enzymes. *Bioelectrochemistry* **132**, 107414 (2020).
8. Bartlett, P. N. & Al-Lolage, F. A. There is no evidence to support literature claims of direct electron transfer (DET) for native glucose oxidase (GOx) at carbon nanotubes or graphene. *J. Electroanal. Chem.* **819**, 26–37 (2018).
9. Bollella, P. & Katz, E. Enzyme-based biosensors: tackling electron transfer issues. *Sensors* **20**, 3517 (2020).
10. Wilson, G. S. Native glucose oxidase does not undergo direct electron transfer. *Biosens. Bioelectron.* **82**, vii–viii (2016).
11. Hecht, H. J., Schomburg, D., Kalisz, H. & Schmid, R. D. The 3D structure of glucose oxidase from *Aspergillus niger*. Implications for the use of GOD as a biosensor enzyme. *Biosens. Bioelectron.* **8**, 197–203 (1993).
12. Hecht, H. J., Kalisz, H. M., Hendle, J., Schmid, R. D. & Schomburg, D. Crystal Structure of Glucose Oxidase from *Aspergillus niger* Refined at 2.3 Å Resolution. *J. Mol. Biol.* **229**, 153–172 (1993).
13. Alvarez-Icaza, M. et al. The design of enzyme sensors based on the enzyme structure. *Biosens. Bioelectron.* **10**, 735–742 (1995).
14. Yu, S. & Myung, N. V. Recent Advances in the Direct Electron Transfer-Enabled Enzymatic Fuel Cells. *Front. Chem.* **8**, 620153 (2021).
15. Cohen, R., Bitton, R. E., Herzallh, N. S., Cohen, Y. & Yehezkeili, O. Utilization of FAD-Glucose Dehydrogenase from *T. emersonii* for Amperometric Biosensing and Biofuel Cell Devices. *Anal. Chem.* **93**, 11585–11591 (2021).
16. Gross, A. J. et al. Diazonium electrografting vs. physical adsorption of Azure A at carbon nanotubes for mediated glucose oxidation with FAD-GDH. *ChemElectroChem* **7**, 4543–4549 (2020).
17. Milton, R. D., Lim, K., Hickey, D. P. & Minter, S. D. Employing FAD-dependent glucose dehydrogenase within a glucose/oxygen enzymatic fuel cell operating in human serum. *Bioelectrochemistry* **106**, 56–63 (2015).
18. Bak, T.-G. Studies on glucose dehydrogenase of *Aspergillus oryzae*. *Biochim. Biophys. Acta (BBA) - Enzymol.* **139**, 277–293 (1967).
19. Filipiak, M. S. et al. Electron transfer from FAD-dependent glucose dehydrogenase to single-sheet graphene electrodes. *Electrochim. Acta* **330**, 134998 (2020).
20. Nakajima, Y. FAD-dependent Glucose Dehydrogenase from *Aspergillus oryzae*. [https://www.wwpdb.org/pdb?id=pdb\\_00007vzp](https://www.wwpdb.org/pdb?id=pdb_00007vzp) [10.2210/pdb7vzp/pdb](https://doi.org/10.2210/pdb7vzp/pdb) (2022).
21. Muguruma, H., Iwasa, H., Hidaka, H., Hiratsuka, A. & Uzawa, H. Mediatorless Direct Electron Transfer between Flavin Adenine Dinucleotide-Dependent Glucose Dehydrogenase and Single-Walled Carbon Nanotubes. *ACS. Catalysis* **7**, 725–734 (2017).
22. Lee, I. et al. The electrochemical behavior of a FAD dependent glucose dehydrogenase with direct electron transfer subunit by immobilization on self-assembled monolayers. *Bioelectrochemistry* **121**, 1–6 (2018).
23. Bernards, D. A. & Malliaras, G. G. Steady-State and Transient Behavior of Organic Electrochemical Transistors. *Adv. Funct. Mater.* **17**, 3538–3544 (2007).
24. Friedlein, J. T., McLeod, R. R. & Rivnay, J. Device physics of organic electrochemical transistors. *Org. Electron.* **63**, 398–414 (2018).
25. Bai, L. et al. Biological applications of organic electrochemical transistors: electrochemical biosensors and electrophysiology recording. *Front. Chem.* **7**, 313 (2019).
26. Sarcina, L. et al. Enzyme based field effect transistor: State-of-the-art and future perspectives. *Electrochem. Sci. Adv.* <https://doi.org/10.1002/elsa.202100216> (2022).
27. Diacci, C. et al. Real-time monitoring of glucose export from isolated chloroplasts using an organic electrochemical transistor. *Adv. Mater. Technol.* **5**, 1900262 (2020).
28. Strakosas, X. et al. Biostack: Nontoxic metabolite detection from live tissue. *Adv. Sci.* **9**, e2101711 (2022).
29. Diacci, C. et al. Diurnal in vivo xylem sap glucose and sucrose monitoring using implantable organic electrochemical transistor sensors. *iScience* **24**, 101966 (2021).
30. Koklu, A. et al. Microfluidics integrated n-type organic electrochemical transistor for metabolite sensing. *Sens. Actuators B: Chem.* **329**, 129251 (2021).
31. Battista, E. et al. Enzymatic sensing with laccase-functionalized textile organic biosensors. *Org. Electron.* **40**, 51–57 (2017).
32. Hitaishi, V. et al. Controlling Redox enzyme orientation at planar electrodes. *Catalysts* **8**, 192 (2018).
33. Strakosas, X. et al. Metabolite-induced in vivo fabrication of substrate-free organic bioelectronics. *Science* **379**, 795–802 (2023).
34. Dufil, G. et al. Enzyme-assisted in vivo polymerisation of conjugated oligomer based conductors. *J. Mater. Chem. B* **8**, 4221–4227 (2020).
35. Priyadarshini, D. et al. Enzymatically polymerized organic conductors on model lipid membranes. *Langmuir* **39**, 8196–8204 (2023).
36. Tommasini, G. et al. Seamless integration of bioelectronic interface in an animal model via in vivo polymerization of conjugated oligomers. *Bioact. Mater.* **10**, 107–116 (2022).
37. Gryszel, M. et al. Vertical organic electrochemical transistor platforms for efficient electropolymerization of thiophene based oligomers. *J. Mater. Chem. C* <https://doi.org/10.1039/D3TC04730J> (2024).
38. Azizian, P., Casals-Terré, J., Ricart, J. & Cabot, J. M. Capillary-driven microfluidics: impacts of 3D manufacturing on bioanalytical devices. *Analyst* **148**, 2657–2675 (2023).
39. Azizian, P., Casals-Terré, J., Ricart, J. & Cabot, J. M. Diffusion-free valve for preprogrammed immunoassay with capillary microfluidics. *Microsyst. Nanoeng.* **9**, 91 (2023).
40. Prabhakar, P. et al. 3D-printed microfluidics and potential biomedical applications. *Front. Nanotechnol.* **3**, 6 (2021).
41. Azizian, P. et al. Coupling Capillary-Driven Microfluidics with Lateral Flow Immunoassay for Signal Enhancement. *Biosensors* **13**, 832 (2023).
42. Schachinger, F., Ma, S. & Ludwig, R. Redox potential of FAD-dependent glucose dehydrogenase. *Electrochem. Commun.* **146**, 107405 (2023).
43. Prinz, H. Hill coefficients, dose–response curves and allosteric mechanisms. *J. Chem. Biol.* **3**, 37–44 (2010).
44. Probst, D. et al. Development of direct electron transfer-type extended gate field effect transistor enzymatic sensors for metabolite detection. *Anal. Chem.* <https://doi.org/10.1021/acs.analchem.3c04599> (2024).
45. Makhinia, A. et al. On-demand inkjet printed hydrophilic coatings for flow control in 3D-printed microfluidic devices embedded with organic electrochemical transistors. *Adv. Mater. Technol.* **8**, 2300127 (2023).
46. Pappa, A. M. et al. Organic transistor arrays integrated with finger-powered microfluidics for multianalyte saliva testing. advanced healthcare. *Materials* **5**, 2295–2302 (2016).
47. Diacci, C. et al. Organic electrochemical transistor Aptasensor for Interleukin-6 Detection. *ACS Appl. Mater. Interfaces* <https://doi.org/10.1021/acsami.3c12397> (2023).
48. Burtscher, B. et al. Functionalization of PEDOT:PSS for aptamer-based sensing of IL6 using organic electrochemical transistors. *npj Biosensing* **1**, 1–8 (2024).

## Acknowledgements

Funding for this project was provided by the European Union's Horizon 2020 research and innovation program under Marie Skłodowska-Curie Grant Agreement No. 813863. (BORGES project). Additional funding was provided

by the Swedish Research Council, the Swedish Foundation for Strategic Research, and the Knut and Alice Wallenberg Foundation.

### Author contributions

B.B. and M.S. characterized OECT devices. C.D. designed, fabricated, and characterized OECT devices. P.A. fabricated and characterized microfluidic devices. T.A. synthesized and characterized tri-thiophene monomers. B.B., C.D., M.S., and T.A. contributed to data collection and figure preparation. J.M.C., X.S., and D.T.S. supervised the research. B.B., P.A., J.M.C., and D.T.S. contributed to the original experimental design. B.B. and P.A. wrote the main manuscript text. J.M.C. and D.T.S. secured funding and resources. All authors contributed to data analysis and figure revision. All authors reviewed the manuscript.

### Funding

Open access funding provided by Linköping University.

### Competing interests

The authors declare no competing interests.

### Additional information

**Supplementary information** The online version contains supplementary material available at <https://doi.org/10.1038/s44328-025-00063-w>.

**Correspondence** and requests for materials should be addressed to Xenofon Strakosas or Daniel T. Simon.

**Reprints and permissions information** is available at <http://www.nature.com/reprints>

**Publisher's note** Springer Nature remains neutral with regard to jurisdictional claims in published maps and institutional affiliations.

**Open Access** This article is licensed under a Creative Commons Attribution 4.0 International License, which permits use, sharing, adaptation, distribution and reproduction in any medium or format, as long as you give appropriate credit to the original author(s) and the source, provide a link to the Creative Commons licence, and indicate if changes were made. The images or other third party material in this article are included in the article's Creative Commons licence, unless indicated otherwise in a credit line to the material. If material is not included in the article's Creative Commons licence and your intended use is not permitted by statutory regulation or exceeds the permitted use, you will need to obtain permission directly from the copyright holder. To view a copy of this licence, visit <http://creativecommons.org/licenses/by/4.0/>.

© The Author(s) 2025